Water–rock interaction in the magmatic-hydrothermal system of Nisyros Island (Greece)

Michele Ambrosio [a], Marco Doveri [b], Maria Teresa Fagioli [a], Luigi Marini [b,c,*], Claudia Principe [b], Brunella Raco [b]

[a] AF Geoscience and Technology Consulting, via Toniolo 222, Campo (PI), 56010, Italy
[b] Institute of Geosciences and Georesources, CNR, Area della Ricerca, Via G. Moruzzi 1, I-56124 Pisa, Italy
[c] Laboratory of Geochemistry, Dip.Te.Ris., University of Genova, Corso Europa 26, I-16132 Genova, Italy

ARTICLE INFO

ABSTRACT

In this work, we investigated the water–rock interaction processes taking place in the hydrothermal reservoir of Nisyros through both: (1) a review of the hydrothermal mineralogy encountered in the deep geothermal borehole Nisyros-2; and (2) a comparison of the analytically-derived redox potentials and acidities of fumarolic-related liquids, with those controlled by redox buffers and pH buffers, involving hydrothermal mineral phases.

The propylitic zone met in the deep geothermal borehole Nisyros-2, from 950 to 1547 m (total depth), is characterised by abundant, well crystallised epidote, adularia, albite, quartz, pyrite, chlorite, and sericite–muscovite, accompanied by less abundant anhydrite, stilpnomelane, wairakite, garnet, tremolite and pyroxene. These hydrothermal minerals were produced in a comparatively wide temperature range, from 230 to 300 °C, approximately. Hydrothermal assemblages are well developed from 950 to 1360 m, whereas they are less developed below this depth, probably due to low permeability.

Based on the R_H values calculated for fumarolic gases and for the deep geothermal fluids of Nisyros-1 and Nisyros-2 wells, redox equilibrium with the $(FeO)/(FeO_{1.5})$ rock buffer appears to be closely attained throughout the hydrothermal reservoir of Nisyros. This conclusion may be easily reconciled with the nearly ubiquitous occurrence of anhydrite and pyrite, since R_H values controlled by coexistence of anhydrite and pyrite can be achieved by gas separation.

The pH of the liquids feeding the fumarolic vents of Stephanos and Polybote Micros craters was computed, by means of the EQ3 code, based on the Cl–δD relationship which is constrained by the seawater–magmatic water mixing occurring at depth in the hydrothermal–magmatic system of Nisyros. The temperature dependence of analytically-derived pH values for the reservoir liquids feeding the fumarolic vents of Stephanos and Polybote Micros craters suggests that some unspecified pH buffer fixes the acidity of these reservoir liquids at values of 4.72–4.85 and 4.88–5.23, respectively. Many of these pH values are lower than those expected for the full-equilibrium condition, although they are close to those of the reservoir liquids of Nisyros-1, 5.16, and Nisyros-2, 4.87. It is likely that this excess of acidity-producing species, chiefly CO_2, promotes release of Fe(II) and Fe(III) to the reservoir liquids through rock dissolution, permitting the attainment of redox equilibrium with the $(FeO)/(FeO_{1.5})$ rock buffer, as already suggested by the late Werner Giggenbach.

© 2010 Elsevier B.V. All rights reserved.

1. Introduction

Nisyros Island is part of the Dodecanese archipelago and it is situated between the islands of Kos and Tilos, near the Turkish coast (see inset in Fig. 1). It has an almost circular shape, an average diameter of 8 km, and a surface area of ca. 42 km². From the geological point of view, Nisyros belongs to the Aegean volcanic arc and is positioned at its easternmost termination, on a thinned crust, with the Moho discontinuity at a depth of ca. 24–27 km (Makris and Stobbe, 1984; Kassaras et al., 2005). The island represents the emerged portion of a complex volcanic edifice built on a limestone basement (Geotermica Italiana, 1983). The volcanic edifice is truncated by a circular 4-km-diameter caldera depression, whose western half is filled by several recent domes.

Today, the occurrence of hydrothermal activity on Nisyros is testified by two types of surface manifestations, namely the thermal
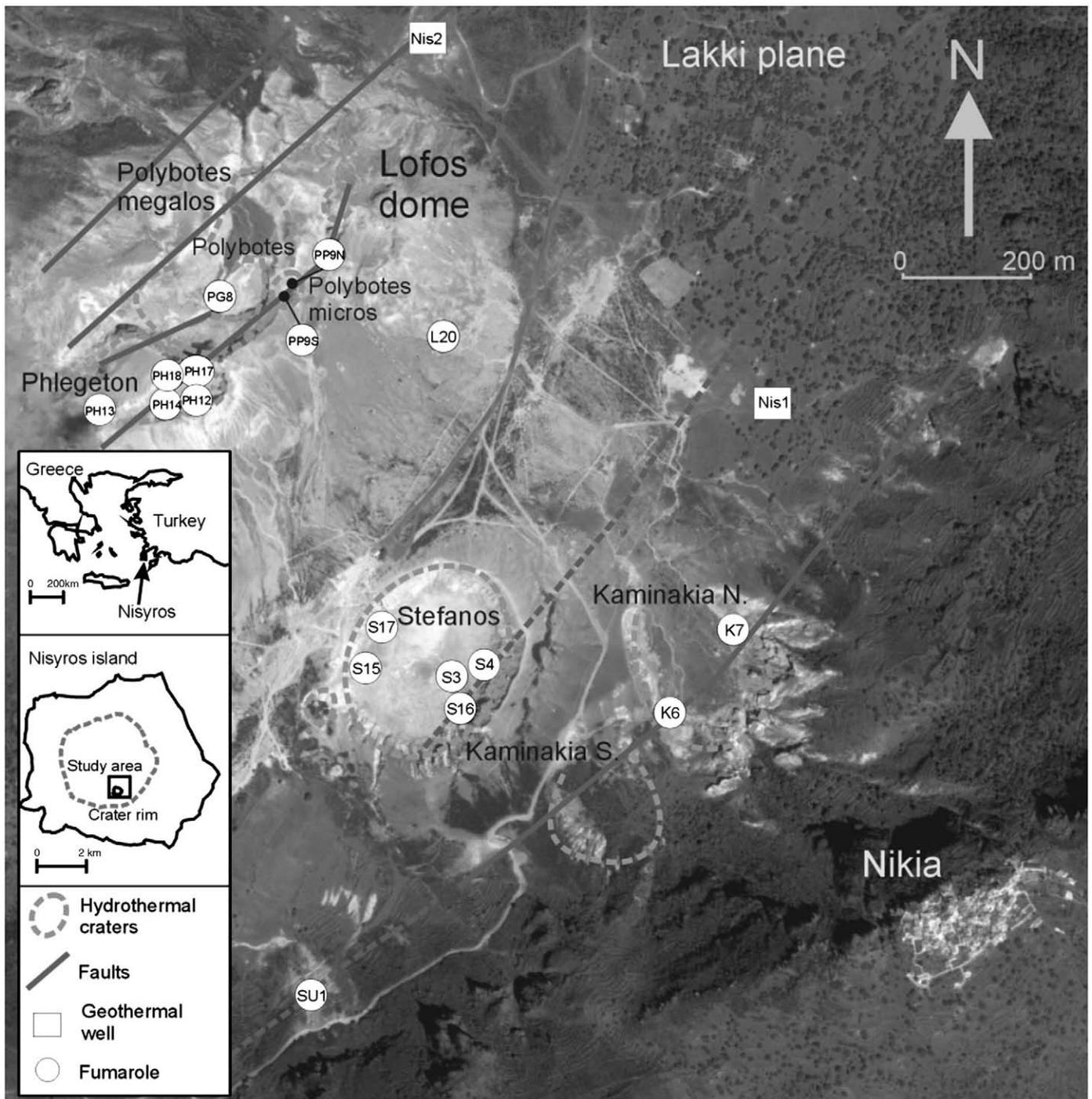
Fig. 1. Location map of hydrothermal craters, fumaroles, and the deep geothermal wells Nisyros-1 and Nisyros-2 (from Chiodini et al., 2002, modified).

springs distributed along the northern and southern coasts of the island (Fig. 2) and the large fumarolic field occupying the southern Lakki plain (Fig. 1). In this area, different hydrothermal eruptions took place in historical times as documented by both several well-preserved hydrothermal craters and the chronicles of M. H. Gorceix and A. Martelli (Marini et al., 1993). Besides, changes in fumarolic chemistry took place in 1995–1998, concurrent with episodes of intense seismicity and ground deformation (Chiodini et al., 2002; Caliro et al., 2005; Shimizu et al., 2005).

Based on the promising results of the geothermal surveys carried out by IGME (the Greek Geological Survey), under the leadership of Giorgio Marinelli, the subsurface of the southern Lakki plain was explored in the '80s by PPC (the Greek Energy Authority). At that time,

the two geothermal wells Nisyros-1 and Nisyros-2 were drilled to total depths of 1816 m and 1547 m, respectively (Geotermica Italiana, 1983; Koutroupis, 1983; Marinelli et al., 1983; Geotermica Italiana, 1984; Vrouzi, 1985).

All the geochemical data available for the fluids circulating in the magmatic-hydrothermal system of Nisyros, including those discharged from the two deep geothermal wells Nisyros-1 and Nisyros-2, the fumaroles of the southern Lakki plain, and the coastal thermal springs, have been compiled and interpreted by Marini and Fiebig (2005). Through this exercise, they elaborated an updated conceptual geochemical model of the magmatic-hydrothermal system of Nisyros (see Section 5), refining that previously proposed by Chiodini et al. (1993a).
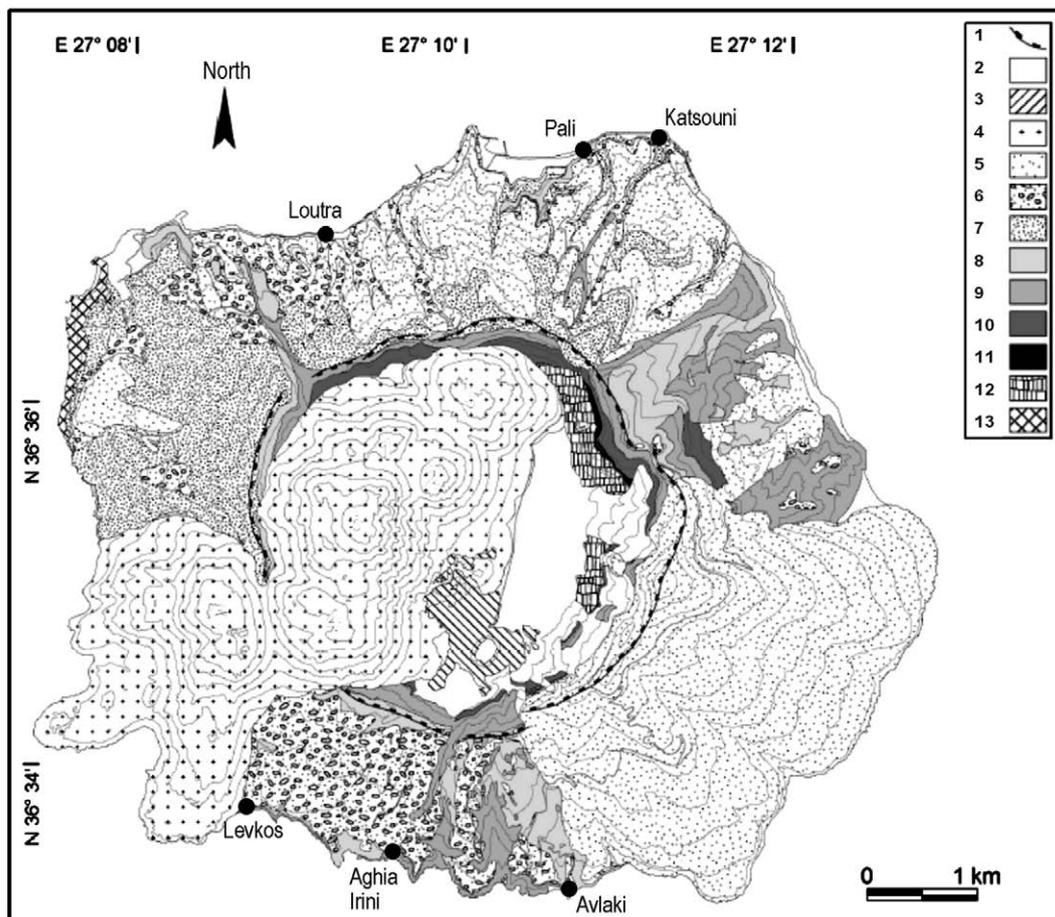
Fig. 2. Simplified geological synthematic map of Nisyros Island, also showing the location of coastal thermal springs (from Volentik et al., 2005a, modified). Symbols as follows: 1 = Morphological caldera rim; 2 = Talus, alluvial, and beach deposits; 3 = Gorceix synthem; 4 = Profitis Ilias synthem; 5 = Palì sub-synthem; 6 = Loutrà sub-synthem; (5 & 6 = Kardià synthem); 7 = Fournià synthem; 8 = Xolante sub-synthem; 9 = Afiònas sub-synthem; (8 & 9 = Liés synthem); 10 = Second-lake sub-synthem; 11 = First-lake sub-synthem; (10 & 11 = Katò Lakkì synthem); 12 = Kremastò synthem; 13 = Kanafià synthem.

This study is aimed at gaining more insights on the water–rock interaction processes occurring in the system of interest, through: (1) a review of the petrographical data on the hydrothermal mineral assemblages encountered in the deep geothermal borehole Nisyros-2; and (2) a comparison of the analytically-derived values of the two main variables governing fluid chemistry, namely redox potential and acidity, with those expected based on active redox buffers and pH buffers, involving hydrothermal minerals.

2. Geological background

After the early geological surveys of the Italian geologists Martelli (1917) and Desio (1931), the geology of Nisyros was mapped by Di Paola (1974), Papanikolaou et al. (1991) and Vougioukalakis (1993). More recently, a totally new geological survey was carried out from 1999 to 2003 by Volentik et al. (2005a,b) who produced a new geological map of Nisyros at the scale 1:12,500 based on the use of the Unconformity Bounded Stratigraphic Units, UBSU (Fig. 2). In this way, lavas, tephra, hydrothermal explosions' deposits, lacustrine sediments, and epiclastites cropping out on Nisyros were classified in 36 cartographic units, distributed in 8 synthems and 6 sub-synthems. Due to the lack of absolute age measurements for Nisyros rocks (Volentik et al., 2005a), the classification in UBSU is particularly important, as it emphasises the discontinuities separating different phases of volcanic activity, the variations in the morphology of the island, and the clustering in time of volcanism, linking volcanic eruptions to other geological events, marked by epiclastic deposits, erosion discontinuities, and lacustrine beds.

Based on the outcomes of previous geological investigations (e.g. Davis, 1967; Keller, 1971; Di Paola, 1974; Vougioukalakis, 1984; Bohla and Keller, 1987; Keller et al., 1990; Limburg and Varekamp, 1991; Papanikolaou et al., 1991; St. Seymour and Vlassopoulos, 1992; Vougioukalakis, 1993; Francalanci et al., 1995; Vougioukalakis, 1998) and newly acquired data, Vanderkluysen et al. (2005a) proposed that the present cone-like morphology of Nisyros island results from the migration of volcanic centres along major tectonic lines (Volentik et al., 2005c) as well as through the periodic reorganization caused by flank collapses and faulting episodes. In particular, an early submarine paleo-volcano was built in the northern sector of the island and experienced an emersion stage followed by re-immersion. Then, several effusive and explosive eruptions lead to the growth of the first truly subaerial cone eastward with respect to the early submarine edifice. This subaerial cone collapsed in response to the Lakki explosive eruption, thus producing the first recognisable summit depression, where a lake settled. Volcanism started again in the same zone causing the construction of a strato-cone, which was partly destroyed by the explosive eruption of Melisserì. This event emitted a large volume of materials that was later reworked on the island. Subsequent volcanic activity, comprising the lava flows of Ellinikà and Argos and the explosive eruption of Stàvros occurred in the northeastern and southern sectors of the island, which acquired a roughly rounded morphology. Then, volcanism took place from scattered centres along the main tectonic trends and resulted in small effusive and explosive events. After a relatively long period of rest, volcanic activity resumed determining the building of a small basaltic andesitic to andesitic cone in the north–west. The subsequent

emplacement of dacitic domes in the north triggered repeated episodes of minor block and ash flows as well as the Vunàri sector collapse, along the northern coast. Then, the explosive eruption of the Lower Pumice, probably fed by a shallow magma chamber, caused the formation of a relatively large caldera near the centre of the island. This was followed by the tectonically-controlled Upper Pumice eruption, with the emission of pyroclastic flows and the construction of a tuff cone. The subsequent rhyodacitic domes of Profitis Ilias, representing the last magmatic event on Nisyros Island, partly filled the caldera depression and partly outpoured westward reaching the sea. The still on-going hydrothermal activity has been already recalled in Section 1.

As recognised by Vanderkluysen et al. (2005b), who reviewed the available petrologic–geochemical information on Nisyros volcanic rocks (Davis, 1967; Di Paola, 1974; Vougioukalakis, 1984; Bohla and Keller, 1987; Lodise, 1987; Wyers and Barton, 1989; Gansecki, 1991; Limburg and Varekamp, 1991; St. Seymour and Vlassopoulos, 1992; Vougioukalakis, 1993; Francalanci et al., 1995; Innocenti et al., 2002; Vanderkluysen and Volentik, 2002; Volentik et al., 2002; Büttner et al., 2005; Pe-Piper and Piper, 2005) and produced new data for selected stratigraphically-positioned samples, Nisyros rocks belong to the calc-alkaline series and span the compositional range from basaltic andesites to rhyolites with a lack of samples between 61 and 63 wt.% SiO_2 (andesite–dacite transition). Fractional crystallisation appears to be the main process controlling the evolution of Nisyros magmas, as pointed out by major elements and traces, apart from the most incompatible traces which cannot be satisfactorily modelled near the andesite–dacite transition. Crystal retention, removal, and re-entrainment as well as magma mingling are suggested by the presence of bimodal crystal populations, quenched mafic enclaves and reversely zoned crystals. In addition, some crustal contamination is indicated by the isotopic data for Sr, Nd, Pb and Hf. Polybaric evolution has been invoked by Wyers and Barton (1989) to account for the different evolution trends of the basaltic andesite–andesite series and of the dacite–rhyolite series, but several open questions remain on the origin of Nisyros magmas, especially the most evolved ones.

3. Subsurface information

Our present perception of the deep geological features of Nisyros Island derives almost in toto from the information obtained through the two geothermal wells Nisyros-1 and Nisyros-2, both situated at the northeastern periphery of the hydrothermal craters' area (Fig. 1). The terrains encountered by the two boreholes are somewhat different in that (Fig. 3): (1) well Nisyros-1 crossed a relatively thin volcanic series and found a comparatively thick pile of carbonate rocks below it, ending into the apophyses of a dioritic intrusion and related thermometamorphic rocks, while (2) well Nisyros-2 crossed a relatively thick volcanic sequence, directly overlying the intrusive-thermometamorphic rocks, whereas no carbonate rocks were met. These differences between the stratigraphic logs of the two boreholes indicate that the caldera depression deepens moving towards its centre.

From the hydrogeological point of view, both boreholes crossed: (1) a shallow permeable zone occurring from 431 to 695 m depth in well Nisyros-1 and from 30 to 365 m depth in well Nisyros-2; and (2) a deep permeable zone extending from 1421 m to well-bottom in well Nisyros-1 and from 1070 to 1360 m in well Nisyros-2. Interestingly, the aquiclude separating the two permeable zones is constituted by the carbonate pile in well Nisyros-1 and by the volcanic succession in well Nisyros-2, confirming that permeability is strictly controlled by the degree of fracturing.

The maximum temperatures, measured in the deepest parts of the two boreholes, are ca. 340 °C in well Nisyros-1 and ca. 320 °C in well Nisyros-2.

During the short-term production tests on well Nisyros-1 it was virtually impossible to obtain representative samples of the reservoir brine owing to precipitation of Na–Ca–K chlorides triggered by steam separation (Marini and Cioni, 1985). Besides, the liquid phases separated at atmospheric pressure showed high contents of Mg^{2+} and SO_4^{2-} ions and low contents of aqueous SiO_2 suggesting the possible entrainment of seawater, which was utilised to make up the drilling mud. The total discharge enthalpy measured for well Nisyros-1 during the short-term production tests, 2340–2360 J/g, is remarkably larger than the enthalpy of pure liquid water at the inferred reservoir temperature (330–335 °C), 1525–1559 J/g (Keenan et al., 1969). This difference indicates the presence of a separate vapour phase in the hydrothermal reservoir and its preferential entrainment in the bi-phase mixture discharged by the well during the short-term production tests.

Both short- and long-term production tests were carried out on well Nisyros-2 and, therefore, the physical and chemical parameters of the reservoir fluid discharged by this well were measured with sufficient precision. The total discharge enthalpy, 1375 ± 25 J/g, is higher than the enthalpy of pure liquid water at the inferred reservoir temperature (290 °C), 1289 J/g (Keenan et al., 1969), by 86 J/g only. This small excess enthalpy suggests the presence in the hydrothermal reservoir, under static conditions, of a single-liquid phase, which becomes a liquid-dominated bi-phase (with a steam fraction $y = 0.058$) under dynamic conditions.

4. Hydrothermal mineral assemblages

The sequence of hydrothermal mineral assemblages found in wells Nisyros-1 and Nisyros-2 is very similar to those found in high-temperature geothermal systems (e.g., Browne, 1970, 1977; Steiner, 1977; Browne, 1982; Kristmannsdottir, 1982; Bird et al., 1984; Heald et al., 1987; Rochelle et al., 1989; Reyes, 1990; Akaku et al., 1991; Milodowski et al., 1992; Reyes et al., 1993). Apart from local variations in the sequence of alteration minerals, a general relationship between hydrothermal alteration minerals and temperature ranges is recognisable, as summarized by Henley and Ellis (1983). The same mineral parageneses were also found in fossil geothermal systems, i.e., in hydrothermal ore deposits. The sequence of hydrothermal mineral assemblages can be divided into several zones, each one characteristic of a distinct temperature range. The transition from one zone to the underlying one is generally gradual, due to the progressive increase in temperature with increasing depth.

The two following sections are largely based on the Geotermica Italiana reports for the two deep geothermal wells Nisyros-1 (Geotermica Italiana, 1983) and Nisyros-2 (Geotermica Italiana, 1984). The hydrothermal mineral deposition in the rock sequences crossed by these two wells is strongly controlled by primary lithologies and permeability. In fact, lavas are generally poorly altered, unless where fractured, while pyroclastic deposits are strongly altered, especially if coarse-grained.

4.1. Hydrothermal minerals in well Nisyros-1

0–300 m — Argillic zone — This zone is characterised by the diffuse presence of clay minerals, indicating temperatures lower than 120–150 °C. From 150 °C the appearance and progressive increase of chlorite mark the transition to the following zone.

301–800 m — Phyllitic zone — Chlorite is abundant throughout this zone, associated with minor amounts of chalcedony, quartz, sericite and zeolites. Pyrite, anhydrite and carbonates are also common. This mineral assemblage is characteristic of temperatures ranging between 150 and 200 °C.

801–1485 m — Hydrothermal minerals are poorly developed within the carbonate sequence. This fact indicates that this unit had originally low permeability (as already recalled in Section 3) since the
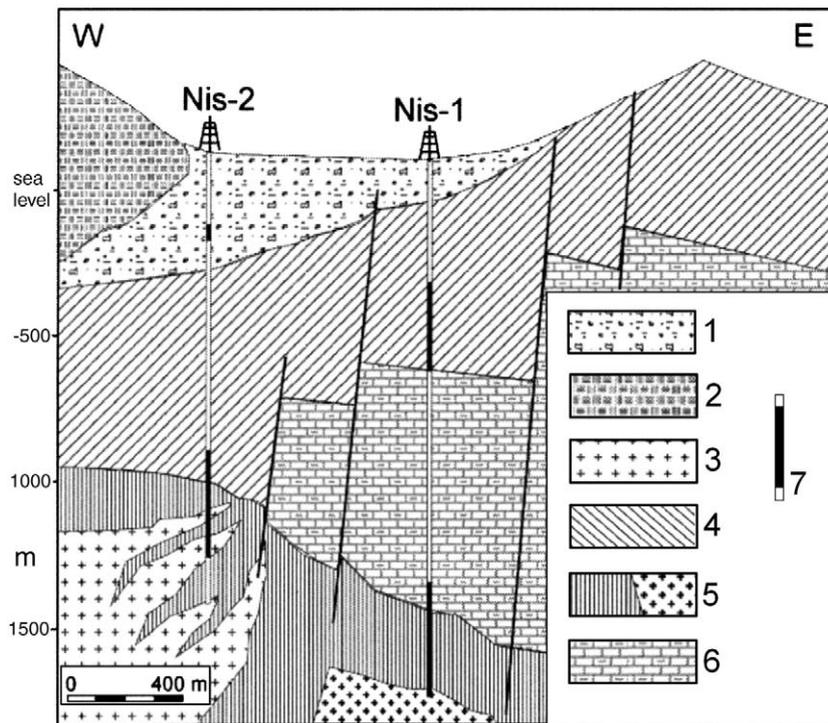
Fig. 3. Geological cross-section through the two deep geothermal wells Nisyros-1 and Nisyros-2 (from Geotermica Italiana, 1984). Symbols as follows: 1 = Talus and alluvial debris filling the caldera depression; 2 = Post-caldera dacitic-rhyodacitic domes; 3 = Subintrusive quartz-dioritic rocks, probably related to post-caldera activity; 4 = Andesitic to dacitic tephra and lavas; 5 = Diorites and thermometamorphic rocks related to the composite volcano magma chamber; 6 = Carbonate rocks and thermometamorphic marbles; 7 = Permeable intervals in geothermal wells.

growth of hydrothermal alteration minerals can occur under active fluid circulation only. However, both the progressive increase in the size of crystal grains within the limestones (from 1000 to 1350 m) and the abundance of pyrite and anhydrite within the underlying marbles indicate a strong and progressive increase in temperature, as well as the input of S-bearing fluids.

1486–1790 m — Propylitic zone — This assemblage develops in the temperature range 230–300 °C and is characterised by abundance of epidote, adularia, albite, tremolite, and pyrrhotite. Also present are: scapolite, brucite, stilpnomelane, quartz, arsenopyrite, pyrite, zeolites (wairakite ?), and garnet. The appearance, at 1680 m, of hydrothermal pyroxene indicates the transition from the propylitic zone to a *contact metamorphic zone*. Pyroxene varies with increasing depth from augite to Fe-hedembergite.

1791–1816 m (total depth) — High K₂O propylitic zone — The presence of biotite and the disappearance of epidote and tremolite are typical of this assemblage, occurring at temperatures higher than 300 °C.

4.2. Hydrothermal minerals in well Nisyros-2

The hydrothermal mineralogy log of well Nisyros-2, in which hydrothermal minerals are arranged according to their behaviour, is shown in Fig. 4.

0–90 m — Argillic zone — This zone is characterised by the presence of clay minerals (kaolinite and montmorillonite) which typically develop at shallow depths under low-temperature conditions.

90–200 m — Argillic–phyllitic zone — This transition zone is marked by the appearance of sericite and chlorite and by the progressive decrease and final disappearance of clay minerals. Temperatures are lower than 120 °C.

200–730 m — Phyllitic–zeolitic zone — The phyllitic zone in well Nisyros-2 is characterised by the presence of sericite, representing the most abundant mineral, while chlorite appears sporadically. Zeolites are widespread in the upper part of the section (above 480 m) and for

this reason this zone has been called *phyllitic–zeolitic*. Quartz, pyrite, anhydrite and carbonates are also common. This hydrothermal assemblage indicates temperatures ranging between 120 and 180 °C.

730–950 m — Phyllitic–propylitic zone — The appearance of microcrystalline epidote marks the transition from the phyllitic zone to the propylitic zone. Albite, sericite and more abundant chlorite together with epidote form the typical assemblage of this zone suggesting temperatures between 180 and 230 °C.

950–1547 m (total depth) — Propylitic zone — The propylitic zone is characterised by abundance of well-crystallised epidote, adularia, albite, quartz, pyrite, chlorite, and sericite–muscovite. Also present are anhydrite, stilpnomelane, wairakite, garnet, tremolite and pyroxene. This assemblage develops at temperatures of 230–300 °C. From 1360 to 1530 m the drilled section does not present a well developed hydrothermal mineral paragenesis, probably due to low permeability.

5. The conceptual geochemical model of the magmatic-hydrothermal system of Nisyros

This section is largely based on the review paper by Marini and Fiebig (2005), to whom the reader is addressed for further details. According to Marini and Fiebig (2005), the conceptual geochemical model of the magmatic-hydrothermal system of Nisyros comprises a degassing magma body (which is situated at unknown depth below the Nisyros caldera) and a hydrothermal aquifer overlying it.

The degassing magma body is probably of rhyodacitic composition and originated mainly through fractional crystallisation from a parent basaltic magma. This degassing rhyodacitic magma batch releases H_2O with a δD value close to −20‰, as typically found along convergent plate margins (Giggenbach, 1992). In addition, magmatic gases contain considerable atomic fractions of radiogenic Ar (from 0.3 to 0.6, based on the data of Shimizu et al., 2005) and have comparatively high $^3He/^4He$ ratios (close to 6.2 Ra or higher; Shimizu et al., 2005), which is also a typical characteristic of this plate–tectonics environment (e.g., Giggenbach and Poreda, 1993; Giggenbach et al., 1993).
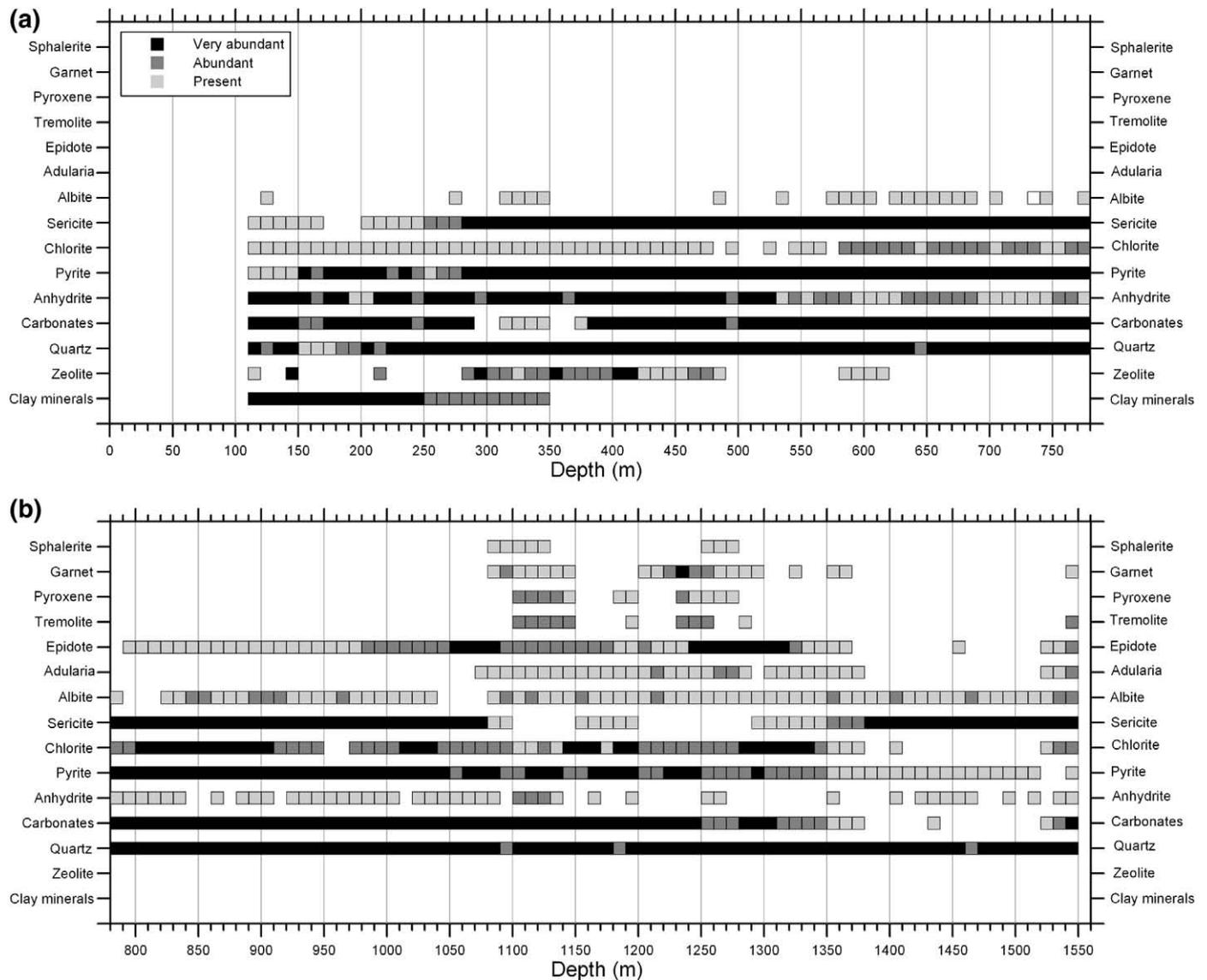
Fig. 4. Log of hydrothermal mineralogy in well Nisyros-2. Low-temperature minerals (clay minerals and low-temperature zeolites) are positioned in the bottom lines. Above are the ubiquitous solid phases, namely quartz, carbonates, anhydrite, pyrite, chlorite and sericite. In the top lines are found the high-temperature minerals, namely albite, adularia, epidote, tremolite, pyroxene, garnet and sphalerite (from Geotermica Italiana, 1984).

Contrary to other island arc systems, the magmatic gases of Nisyros are N$_2$-poor, with respect to He and Ar, probably due to scarcity of N-rich sediments in the subducted slab (Giggenbach, 1996). In line with this hypothesis, both the contribution of CO$_2$ originated by thermal decay of sedimentary organic substances (evaluated as suggested by Sano and Marty, 1995) and the supply of S from biogenic sulfides in subducted sediments (Marini et al., 2002) are also virtually nil or undetectable.

The gases released from the degassing magma batch enter the overlying hydrothermal aquifer from below, thus supplying both heat and chemical substances to it, including H$_2$O, CO$_2$, SO$_2$, H$_2$S, HCl, HF, etc. In addition to arc-type magmatic water, the Nisyros hydrothermal aquifer receives a significant contribution of seawater, whereas the meteoric water supply is nil or negligible (Marini et al., 2002; Brombach et al., 2003). Under the hydrothermal craters of Stephanos and Polybotes, the contribution of arc-type magmatic water is close to 75%, while the remaining 25% is water of marine provenance. The liquid discharged by the geothermal well Nisyros-2 can be considered to be either a mixture made up of ~37% of arc-type magmatic water plus ~63% of local seawater or a mixture made up of ~50% of parent hydrothermal liquid and ~50% of local sea water (Marini and Fiebig,

2005; Dotsika et al., 2009). The magmatic contribution decreases further and the seawater contribution increases correspondingly moving towards the peripheral parts of the hydrothermal craters' area, that is towards Kaminakia and Phlegeton. Although the maximum magmatic contribution may appear very high, it is similar to that detected at Montserrat in 1991–1992 (Chiodini et al., 1996), few years before the onset of the magmatic eruption which begun in September 1995.

The maximum temperature of the deep hydrothermal aquifer is close to 340 °C or somewhat higher, as suggested by both the geochemical thermometry of fumarolic fluids and the CO$_2$/CH$_4$ fractionation of C isotopes (Fiebig et al., 2004). The hydrothermal reservoir hosts brines with Cl contents up to 75,500–78,900 mg/kg, as indicated by the chloride plots of δD and $\delta^{18}O$ values, which are chiefly constrained by local seawater and the Nisyros-2 reservoir liquid (Cl = 50,390 mg/kg; Chiodini et al., 1993a; $\delta D = -1.8‰$; $\delta^{18}O = +3.5‰$; isotopic data from Dotsika, 1992).

Below the hydrothermal craters' area, the deep hydrothermal liquids rise up towards the surface, along fractures and faults, experience heat loss through conduction and cool from the initial reservoir temperatures to 195–284 °C. Then, the deep hydrothermal

liquids boil and the vapours (separated at $T_S = 195–271\ °C$) discharge at the surface after experiencing either negligible condensation (as in the case of Stephanos and Polybotes Micros fumaroles) or significant condensation (as in the case of Kaminakia fumaroles). Assuming a vapour-static regime from the surface to the vapour/liquid separation zone, the depth of this zone is estimated to vary from 490 m for $T_S = 195\ °C$ to 765 m for $T_S = 271\ °C$.

In addition to the vapour flow emitted from the fumarolic vents, another vapour flux, even more important, rises up towards the surface in the hydrothermal craters' area and nearby sectors of the Lakki plain, as indicated to by the elevated CO_2 fluxes from soil and high soil temperatures measured in this area (Brombach et al., 2001; Caliro et al., 2005) by means of the accumulation chamber method (Chiodini et al., 1998). Most water vapour condenses near the surface, whereas both CO_2 and heat are released to the atmosphere, similar to what observed in other fumarolic areas (e.g., Chiodini et al., 2001). According to Caliro et al. (2005), a total hydrothermal CO_2 output of 67.8 t/d is emitted from a total area of 2.1 km². This CO_2 is accompanied by a flux of water vapour of 1420 t/d (16 kg/s) and a heat flux of 42.5 MW. Below the hydrothermal craters' area, this considerable flow of water vapour forms a sort of irregular column, whose shape is constrained by fractures and faults. Therefore, contrary to what was proposed by Chiodini et al. (1993a), the shallow aquifer is absent in this area. However, the shallow aquifer, with maximum temperatures of 120–180 °C, is present in adjacent areas, as testified by the deep geothermal wells Nisyros-1 and Nisyros-2 (see Section 3).

For what concerns the vapour condensate, part of it infiltrates at depth, part of it is re-entrained in the uprising vapour flow and part of it flows from the hydrothermal craters' area towards the northern and southern coasts of the island, contributing to feed the thermal springs. In fact, these thermal waters have chemistry similar to that of seawater and originate through addition of fumarolic vapour and/or vapour condensate to local seawater which infiltrates inland and reacts with volcanic rocks. Consistent with this hypothesis, the average equilibrium temperature of these thermal waters is close to 100 °C (based on anhydrite saturation) − 120 °C (based on the K–Mg geothermometer).

6. Water–rock interaction in the hydrothermal reservoir of Nisyros

With the ultimate aim to gain insights into the water–rock interaction processes occurring in the hydrothermal reservoir of Nisyros, the following discussion is focussed on redox potential and acidity, which are the two main variables governing fluid chemistry, in addition to temperature and pressure. Our analysis is largely based on the theoretical approach of Werner F. Giggenbach, outlined in a series of ground breaking scientific papers (Giggenbach, 1980, 1984, 1987, 1988, 1992, 1993, 1996, 1997).

6.1. Processes governing the redox potential

As shown by Giggenbach (1987), through an exhaustive investigation on the redox processes controlling the chemistry of volcanic gases, the most active redox species is H_2. Its fugacity was utilised, together with the fugacity of water, to define the variable

$$R_H = \log \left(f_{H_2} / f_{H_2O} \right), \tag{1}$$

which can be approximated as $R_H \cong \log(x_{H_2}/x_{H_2O})$, where x_i is the mol fraction of the i-th gas species, as long as the ratio between the fugacity coefficients of H_2 and H_2O does not diverge significantly from

unity. Starting from the analytical results, it is a simple matter to compute the R_H values for the corresponding hypothetical equilibrium vapours, taking into account the distribution of gas species between coexisting vapour and liquid phases (e.g., Chiodini and Marini, 1998). Values of R_H can also be easily converted into the fugacity of oxygen, by means of the following relation (T in K):

$$\log f_{O_2} = -2 \cdot R_H + 5.224 - 25432 / T, \tag{2}$$

which is obtained rearranging the log K of the dissociation reaction of water vapour in hydrogen and oxygen:

$$2H_2O_{(g)} = 2\ H_{2(g)} + O_{2(g)} \tag{3}$$

and taking into account the thermodynamic data stored in SUPCRT92 (Johnson et al., 1992). However, as underscored by Giggenbach (1987), f_{O_2} is not a very useful variable below 350 °C approximately, as equilibrium O_2 concentrations are much lower than measurable values, whereas R_H is still determinable and consequently meaningful.

According to Giggenbach (1987), the two main redox buffers acting in magmatic-hydrothermal environments are:

(1) The rock buffer, corresponding to a nearly constant R_H value of −2.82 at all temperatures of interest, which is controlled by the equilibrium between the aqueous fluid and rocks containing bivalent and trivalent iron in nearly equal quantities, as unspecific (FeO) and (FeO$_{1.5}$), respectively.

(2) The magmatic gas buffer, involving H_2S and SO_2, the two main S species present in magmatic fluids, again in similar amounts, to offer the optimum buffer capacity.
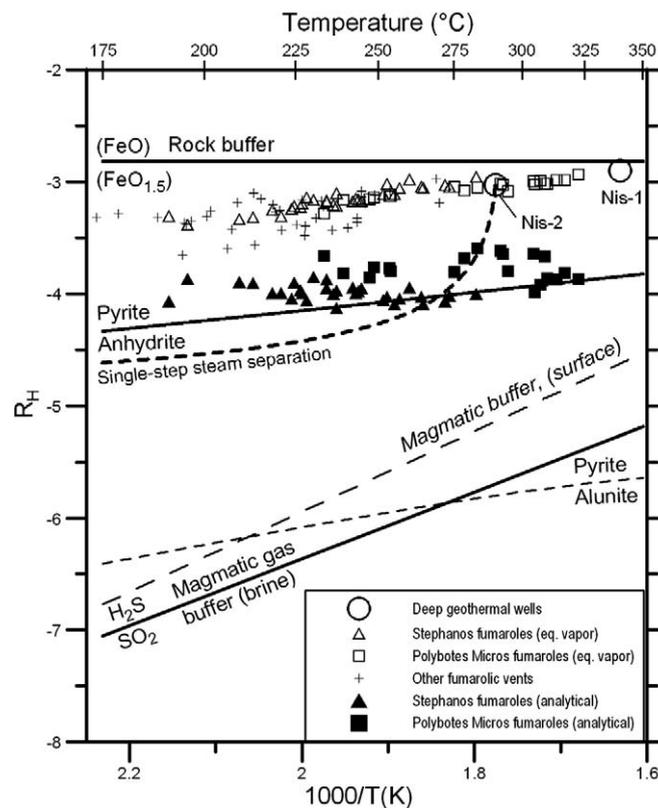
Fig. 5. Values of R_H as a function of temperature for the liquid phases tapped by the deep geothermal wells Nisyros-1 and Nisyros-2 as well as those feeding the fumarolic vents of the hydrothermal craters' area. Also shown are both different redox buffers acting in hydrothermal–magmatic environments and the effects of single-step steam separation on the Nisyros-2 liquid phase (from Giggenbach, 1987, modified).

The R_H values dictated by these two buffers at different temperatures, in the 175–350 °C interval, are shown in Fig. 5. Two different lines are drawn for the magmatic gas buffer. One (labelled 'brine') refers to f_{H_2O} values controlled by boiling aqueous solutions of increasingly high salinities with increasing temperatures, as defined by the equation (Giggenbach, 1987):

$$\log f_{H_2O} = -1820 / T + 4.900, \tag{4}$$

which holds up to 600 °C approximately. The other line (labelled 'surface') refers to f_{H_2O} equal to atmospheric pressure. Inspection of Fig. 5 suggests that magmatic gases become progressively oxidising during cooling, if they follow any unspecified, intermediate path between these two lines. The possibility of the sulphur redox couple to be active throughout its cooling pathway largely depends on the interaction with external (non-magmatic) water bodies. In the dry, vapour-dominated environments present above a degassing magma batch (such as at White Island and Vulcano Island as shown by Giggenbach, 1987, Chiodini et al. 1993b, and Chiodini et al., 1995), the magmatic buffer remains totally active until the surface. In contrast, equilibrium with the rock buffer may be approached and possibly attained, where magmatic gases enter the roots of a liquid-dominated hydrothermal system, as in the case of Nisyros. Consistent with these expectations, all the fluid samples representative of the hydrothermal reservoir of Nisyros, including the liquid phases tapped by the deep geothermal wells Nisyros-1 and Nisyros-2 as well as those feeding the fumarolic vents of the hydrothermal craters' area, distribute close to the rock buffer, in line with previous findings by Chiodini and Marini (1998), Brombach et al. (2003) and Marini and Fiebig (2005).

Also shown in Fig. 5 are two other redox buffers, one is constrained by coexistence of pyrite and alunite and intersects the magmatic gas buffer, the other is controlled by pyrite and anhydrite and is situated half way between the two major redox buffers recognised by Giggenbach (1987). Both the pyrite/alunite and the pyrite/anhydrite buffers may be important at some intermediate stage during the evolution of initially magmatic fluids. For taking into account the processes controlling redox conditions in liquid-dominated hydrothermal systems, it must be recalled first that absorption of magmatic gases into deep waters brings about the production of acidic, highly reactive aqueous solutions. In these environments, sulphur dioxide disproportionates into H_2S and sulphate species, comprising SO_4^{2-}, HSO_4^- and H_2SO_4, whose mutual proportions are dictated by pH (Murray and Cubicciotti, 1983). Taking bisulphate ion as the prevailing sulphate species, the reaction can be written as follows:

$$4\ SO_{2(aq)} + 4\ H_2O_{(l)} \rightarrow H_2S_{(aq)} + 3\ HSO_4^-\ (aq) + 3H^+. \tag{5}$$

Consequently, redox conditions are governed by coexisting aqueous sulphide and sulphate species instead of dissolved SO_2, whose concentration becomes negligible small. Low R_H values are expected, therefore, in deep, highly reactive aqueous solutions.

Water–rock interaction and partial neutralisation of acid-generating species may determine the precipitation of mineral phases, such as alunite [$KAl_3(SO_4)_2(OH)_6$], pyrite [FeS_2], illite [$K_{0.8}Al_{2.8}Si_{3.2}O_{10}(OH)_2$], goethite [$FeOOH$], pyrophyllite [$Al_2Si_4O_{10}(OH)_2$] and chalcedony [$SiO_2$] whose coexistence acts as a redox buffer, as indicated by the reaction:

$$2\ FeS_2 + 2.5\ K_{0.8}Al_{2.8}Si_{3.2}O_{10}(OH)_2 + 15\ H_2O_{(g)} + 5\ H_2O_{(l)} \tag{6}$$

$$= 2\ KAl_3(SO_4)_2(OH)_6 + 0.5\ Al_2Si_4O_{10}(OH)_2 + 2\ FeOOH$$

$$+ 6\ SiO_2 + 15\ H_{2(g)}.$$
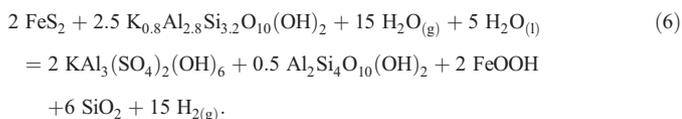
Owing to the low R_H values, corresponding to highly oxidising conditions, bivalent iron leached from the rock is oxidised to ferric ion, which is assumed to precipitate as goethite. To balance the K^+ ion

stored in alunite, formation of illite is hypothesised, which is a reasonable assumption in not too acidic environments. In any case, the position of the alunite/pyrite buffer in Fig. 5 is strictly controlled by redox-active species, namely pyrite, alunite and gaseous hydrogen, whereas it makes little difference to choose as reaction partners: (1) a distinct K-bearing Al-silicate (e.g., muscovite or K-feldspar) instead of illite, (2) a cation-free silicate of Al other than pyrophyllite (e.g., kaolinite or halloysite); and (3) an Fe(III)-mineral with a degree of hydration different from the oxy-hydroxide goethite, either water-free hematite [Fe_2O_3] or the water-rich ferric hydroxide [$Fe(OH)_3$].

Upon further rock dissolution and neutralisation of acid-producing species, the R_H value is expected to increase considerably, causing disappearance of alunite and stabilisation of anhydrite as major sulphate mineral. The redox buffer constituted by coexisting anhydrite and pyrite is expected to be particularly important in the hydrothermal–magmatic system of Nisyros, in which both minerals are almost ubiquitous, even in the hydrothermal reservoir (see Section 4). Similar to Nisyros, widespread distribution of anhydrite and pyrite was also found in the Miravalles geothermal system, Costa Rica (Rochelle et al., 1989; Milodowski et al., 1992), where well-equilibrated, neutral Na–Cl aqueous solutions prevail in the reservoir, although immature, acidic Na–Cl–SO₄ liquids are locally present (Marini et al., 2003a).

The pyrite/anhydrite boundary in Fig. 5 was calculated on the basis of the reaction:

$$2\ FeS_2 + 4\ Ca_2Al_3Si_3O_{12}(OH) + 4\ KAlSi_3O_8 + 15\ H_2O_{(g)} + 3\ H_2O_{(l)} \tag{7}$$

$$= 4\ KAl_3Si_3O_{10}(OH)_2 + 4\ CaSO_4 + 2\ Ca_2FeAl_2Si_3O_{12}(OH)$$

$$+ 6\ SiO_2 + 15\ H_{2(g)}.$$
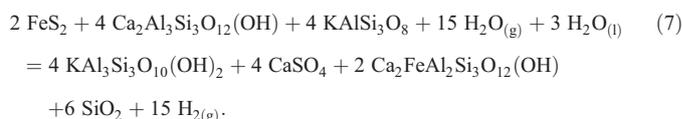
which includes, *inter alias*, clinozoisite [$Ca_2Al_3Si_3O_{12}(OH)$] on the left side and epidote [$Ca_2FeAl_2Si_3O_{12}(OH)$] on the right side. Reaction (7), therefore, takes into account, at least to a certain degree, the compositional changes in clinozoisite–pistacite solid mixtures. Reaction (7) is somewhat different from that suggested by Giggenbach (1997):

$$2\ FeS_2 + 4\ Ca-Al_2 - silicate + nH_2O \tag{8}$$

$$= 4CaSO_4 + Fe_2O_3 + 4\ Al_2 - silicate + 15\ H_2.$$
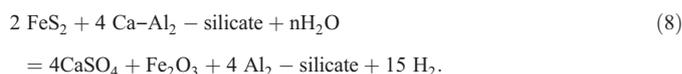
As Giggenbach (1997) considered a very large temperature range (from 100 to 600 °C), reaction (8) was specifically designed to involve different Ca–Al₂-silicates, namely laumontite at temperatures up to 240 °C, followed by wairakite, and anorthite above 350 °C. For the same reason, the Al₂-silicate was considered to be kaolinite up to 240 °C, then pyrophyllite. These variabilities reflect in the stoichiometric coefficient of water, which is unspecified in reaction (8). In spite of these differences, both reactions (7) and (8) have essentially the meaning of pyrite/anhydrite redox boundary and their corresponding lines are not so different in Fig. 5.

Further water–rock interaction and neutralisation of acid-promoting species may finally lead to attainment of full equilibrium between a fluid and its host rock, as detailed in the following section. According to Giggenbach (1997), in fully equilibrated systems, all magmatic-derived, redox-active species are present in the aqueous solution in very low contents. Consequently, redox conditions are governed by bivalent and trivalent iron of the rock, upon its release to the aqueous phase. Close attainment of redox equilibrium with the $(FeO)/(FeO_{1.5})$ rock buffer seem to occur in the single-liquid phase hosted into the hydrothermal reservoir of Nisyros, as suggested by all the available fluid samples, as already noted above. The apparent contrast between these findings and the widespread occurrence of anhydrite and pyrite can be attributed to the action of gas loss. In fact, analytical R_H data for Stephanos and Polybotes Micros fumarolic fluids (which are representative of the boiling liquid phases whose separated vapours are discharged by these

fumarolic vents) plot close to the anhydrite–pyrite buffer. This is not surprising as progressive steam separation causes a gradual decrease in the R_H value, as indicated by the 'single-step steam separation' line drawn in Fig. 5, which was computed following the approach of Giggenbach (1980) and Chiodini and Marini (1998). In other terms, boiling pushes the aqueous system towards relatively oxidising redox conditions, closely approximated by the anhydrite–pyrite mineral buffer.

6.2. Processes governing the acidity

The usually selected variable to define the acidity of aqueous solutions is pH, the negative decadic logarithm of hydrogen ion activity, although its usefulness at high temperatures is questionable as it cannot be directly determined (Giggenbach, 1997). In addition, even the so-called *strong* acids become more and more associated with increasing temperatures, thus causing a reduction in hydrogen ion activity. In spite of these obvious limitations, we will keep pH as the reference variable to investigate the processes governing the acidity of the fluids hosted in the hydrothermal–magmatic system of Nisyros.

As discussed in the previous section, absorption of magmatic gases into deep groundwaters generates acidic, strongly reactive aqueous solutions which are progressive neutralised through water–rock interaction. During this progressive neutralisation, a plethora of pH buffers becomes active as shown by reaction path modelling (e.g., Reed, 1997; Symonds et al., 2001; Marini et al., 2003a,b; Marini and Gambardella, 2005), which is a powerful geochemical tool originally proposed by Helgeson and coworkers (e.g., Helgeson, 1968; Helgeson et al., 1969). Trying to maintain the following discussion to a reasonably simple level, only two of these pH buffers are represented in

Fig. 6. Values of pH as a function of temperature for the liquid phases tapped by the deep geothermal wells Nisyros-1 and Nisyros-2 as well as for the liquids feeding the fumarolic vents of the hydrothermal craters' area. Also shown are an acidic pH buffer (controlled by coexistence of alunite, chalcedony, goethite, illite, pyrite and pyrophyllite) and the full-equilibrium pH buffer, both for chloride concentrations of Nisyros magmatic water (MW), Nisyros-2 liquid phase (Nis-2) and seawater (SW), as well as the effects of single-step steam separation on the Nisyros-2 liquid phase.

Fig. 6. One is an acidic pH buffer governed by coexistence of alunite, chalcedony, goethite, illite, pyrite and pyrophyllite, the other one is the full-equilibrium pH buffer. Since the values of pH buffers depend on both temperature and the concentrations of mobile dissolved constituents, chiefly chloride, the theoretical pH-temperature curves pertinent to both selected buffers were calculated for fixed chloride contents of 19353 mg/kg (average seawater, Nordstrom et al., 1979), 50390 mg/kg (reservoir liquid of Nisyros-2 well, Chiodini et al., 1993a), and 94850 mg/kg (magmatic water of Nisyros, Marini et al., 2002; Brombach et al., 2003; Marini and Fiebig, 2005) and variable temperatures, at step of 25 °C, by means of the EQ3 code, version 8.0 (Wolery and Jarek, 2003).

It must be recalled that the full-equilibrium condition between a fluid and its host rock represents the final state of interaction in a rock-dominated system (Giggenbach, 1984). The secondary minerals represent the thermodynamically stable solid products, generated through water–rock interaction, and containing all the chemical constituents of the primary rock. This secondary mineral assemblage is independent of the chemistry of the initial rock, as long as it is not too different from that of the average crust. In the full-equilibrium assemblage, Na is accommodated in albite [$NaAlSi_3O_8$], K and excess Al in the pair K-feldspar [$KAlSi_3O_8$] plus muscovite [$KAl_3Si_3O_{10}(OH)_2$], Mg in 14 Å-clinochlore [$Mg_5Al_2Si_3O_{10}(OH)_8$] up to 300 °C and biotite at higher temperatures, whereas Ca enters different minerals, namely either laumontite [$CaAl_2Si_4O_{12} \cdot 4H_2O$] or epidote [$Ca_2FeAl_2Si_3O_{12}$ (OH)] or wairakite [$CaAl_2Si_4O_{10}(OH)_4$], depending on temperature. Chalcedony (i.e., microcrystalline quartz), calcite [$CaCO_3$], fluorite [CaF_2], pyrite and anhydrite (following Guidi et al., 1990 and Chiodini et al., 1991) are also part of the full-equilibrium assemblage. Most if not all these minerals are typical components of the propylitic hydrothermal assemblage (see Section 4).

The effects of single-step steam separation on the Nisyros-2 liquid phase are also represented in Fig. 6. Loss of acidic gas species (mainly CO_2) causes a substantial increase in pH, which may attain values higher than expected for the full-equilibrium condition.

In addition to these theoretical curves, also shown in Fig. 6 are the pH, temperature values for the liquid phases tapped by the deep geothermal wells Nisyros-1 and Nisyros-2 (data from Chiodini et al., 1993a) as well as for the liquids feeding the fumarolic vents of Stephanos and Polybote Micros craters (see location in Fig. 1) through steam separation. The pH values for these fumarolic-related liquids were computed in this study, through the following procedure. First, the Cl contents of these liquid phases ($Cl_{L,0}$ in mg/kg) were obtained by inserting the δD values of these fumarolic-related liquids ($\delta D_{L,0}$ in ‰ vs. V-SMOW; data reported by Marini and Fiebig, 2005) in the following equation:

$$Cl_{L,0} = -2514 \cdot \delta D_{L,0} + 44575. \tag{9}$$

Eq. (9) describes to a first approximation the deep mixing process involving seawater and magmatic water, which occurs in the roots of the hydrothermal–magmatic system of Nisyros (Marini et al., 2002; Brombach et al., 2003; Marini and Fiebig, 2005). Then, the CO_2 and H_2S mol fractions in the liquids of interest ($x_{i,L,0}$) were calculated through the relation:

$$x_{i,L,0} = x_{i,V} \cdot \left(s + \frac{1-s}{B_{i,T_s}} \right) \tag{10}$$

where $x_{i,V}$ is the measured mol fraction of the i-th species in the fumarolic vapour, s is the steam fraction and $B_{i,T_s} \cong x_{i,V}/x_{i,L}$ is the vapour–liquid distribution coefficient of the i-th species at the separation temperature T_s. The mol fractions of CO_2 and H_2S in the fumarolic vapours and the values of s and T_s reported by Marini

and Fiebig (2005) were inserted in Eq. (10). Fugacities of CO_2 and H_2S were then calculated through the relation:

$$f_i = K_{H,i} \cdot x_{i,L,0} \tag{11}$$

where $K_{H,i}$ is the Henry's constant (on the mol fraction scale) for the solubility of the i-th species in pure water. The vapour–liquid distribution coefficients of CO_2 and H_2S were obtained from the Henry's constants reported in the thermodynamic database of EQ3/6, $K_{H,i}$ (suitably converted to the mol fraction scale), and P_{H_2O}, by using the equation:

$$B_i = K_{H,i} / P_{H_2O}. \tag{12}$$

Finally, the pH of each aqueous solution was computed by means of EQ3 assuming that: (1) Na molality is equal to Cl molality; and (2) concentrations of dissolved carbonate and dissolved sulphide are fixed by CO_2 and H_2S fugacities. A negligible concentration (10^{-20} mol/kg) was assigned to dissolved sulphate, the strict basis species of S. The O_2 fugacity corresponding to the R_H value (Eq. (2)) was imposed as redox constraint. Electrical balancing on H^+ was selected, to instruct the code to compute the pH of the aqueous solution. Individual activity coefficients of charged solutes were calculated by means of the Debye–Hückel expression with the B-dot extension term, although the ionic strength of the considered aqueous solutions is somewhat higher than the maximum value normally suggested for use of this equation, 1 mol/kg at most (e.g., Wolery and Jarek, 2003).

Fig. 6 shows that the computed pH values for the fumarolic-related liquids vary regularly with temperature, similar to the theoretical pH buffers, suggesting that some unknown buffer systems likely control the acidity of these liquids. In addition, the Stephanos liquid exhibits the lowest pH values varying between 4.72 and 4.85, whereas the Polybotes Micros liquid has higher pH values, oscillating between 4.88 and 5.23. All these pH values are substantially similar to those of the reservoir liquids tapped by wells Nisyros-1, 5.16, and Nisyros-2, 4.87. Comparison with the full-equilibrium curves shows that these analytically-derived pH values are somewhat lower than those expected for the full-equilibrium buffer, for the Nisyros-2 liquid, the Stephanos liquid, and the low-temperature Polybotes Micros liquid. On the other hand, analytically-based pH's are comparable with full-equilibrium pH's, for the Nisyros-1 liquid and the high-temperature Polybotes Micros liquid.

These findings, especially the comparatively low pH values of the Nisyros-2 liquid, the Stephanos liquid, and the low-temperature Polybotes Micros liquid (taking the full equilibrium as theoretical reference) appear to be in contrast with the close attainment of redox equilibrium with the $(FeO)/(FeO_{1.5})$ rock buffer throughout the hydrothermal reservoir of Nisyros. To explain this discrepancy, it must be recalled that readjustment of the redox potential depends on the release to the aqueous solution of bivalent and trivalent iron through rock dissolution and, consequently, on the availability of acidity-producing species. Where acidity-generating species are readily available, their action can promote the release of large quantities of redox-active components from the rocks and the consequent attainment of redox equilibrium, whereas the aqueous solution may still appear to be immature with respect to acidity. These conditions, already recognised for the hydrothermal systems associated with active volcanoes in the Philippines (Giggenbach, 1993; Reyes et al., 1993), may apply to the Nisyros hydrothermal–magmatic system as well. Accepting this interpretation, the pivotal role in water–rock interaction of CO_2, the major acidity-producing component below 400 °C (Giggenbach, 1997), is highlighted once again.

6.3. A final warning

It must be underscored that the interpretation proposed above on the processes governing the redox potential and the acidity of the aqueous solutions circulating in the geothermal reservoir of Nisyros is largely built on gas geothermometry, especially on the interpretation of CO re-equilibration (e.g., Chiodini et al., 2002; Brombach et al., 2003; Fiebig et al., 2004; Marini and Fiebig, 2005). On the one hand, H_2 geothermometers (based on the H_2/H_2O, H_2/Ar, and H_2/N_2 ratios) and CH_4 geothermometers (i.e., the CH_4/CO_2 ratio and the exchange of C isotopes between CH_4 and CO_2) suggest equilibrium temperatures close to the maximum temperature physically measured in the deepest part of borehole Nisyros-1, i.e., 340 °C approximately. These results, provided by the gases discharged by all the fumarolic vents, apart from those of Kaminakia, indicate the provenance of these gases from a single-liquid phase with this initial temperature. On the other hand, CO-based geothermometers suggest equilibration of this gas species in a single-liquid phase at 195 to 284 °C, followed by steam separation at 195–271 °C (although CO equilibration in separated vapours cannot be ruled out; Chiodini et al., 2002). A possible way to reconcile these different temperatures of gas equilibration in a single-liquid phase (~340 °C for H_2 and CH_4 vs. 195–284 °C for CO) is to assume that the uprising deep hydrothermal liquids experience conductive cooling, as proposed by previous authors (see Section 5).

To substantiate this interpretation it must be recalled that: (1) CO re-equilibration proceeds fast at 240–350 °C in a liquid phase, where different dissolved species may act as catalysts for the water–gas shift reaction:

$$CO + H_2O \rightarrow CO_2 + H_2, \tag{13}$$

which was discovered by the Italian physicist Felice Fontana in 1780, whereas (2) as soon as a vapour phase forms, gases transfer almost completely into it and carbon monoxide quenches, as suggested by CO behaviour in the fumarolic gases of Vulcano (Chiodini et al., 1993b).

Of course, it cannot be totally excluded (similar to all geothermometric applications) that equilibrium temperatures and separation temperatures suggested by CO are meaningless. If so, the only meaningful equilibrium temperatures would be those indicated by H_2 and CH_4, although we consider this as a highly unlikely possibility.

7. Conclusions

The effects of the water–rock interaction processes occurring in the hydrothermal reservoir of Nisyros were investigated through both: (1) a review of the petrographical data available for the hydrothermal mineral assemblages met in the deep geothermal well Nisyros-2; and (2) a comparison of the analytically-derived values of the two main variables governing fluid chemistry, namely redox potential and acidity, with those expected on the basis of redox buffers and pH buffers involving hydrothermal minerals.

In the deep geothermal well Nisyros-2, the propylitic zone extends from 950 to 1547 m (total depth) and is marked by abundance of well crystallised epidote, adularia, albite, quartz, pyrite, chlorite, and sericite–muscovite. This prevailing mineralogy is accompanied by less abundant anhydrite, stilpnomelane, wairakite, garnet, tremolite and pyroxene. All these minerals formed in a relatively large temperature interval, from 230 to 300 °C, approximately. Hydrothermal minerals are well developed from 950 to 1360 m, whereas they are less developed below 1360 m, probably due to low permeability.

To study the distribution of redox potential in reservoir fluids, R_H values were computed for all the fumarolic analyses reported by Marini and Fiebig (2005), considering the distribution of gas species between coexisting vapour and liquid phases (e.g., Chiodini and Marini, 1998). All the fluid samples representative of the hydrothermal reservoir of Nisyros, comprising the liquid phases encountered by the deep

geothermal wells Nisyros-1 and Nisyros-2 as well as those feeding the fumarolic vents of the hydrothermal craters' area, distribute close to the $(FeO)/(FeO_{1.5})$ rock buffer, as already noted by Chiodini and Marini (1998), Brombach et al. (2003) and Marini and Fiebig (2005). These findings are in apparent contrast with the widespread occurrence of anhydrite and pyrite, which are abundant even in the hydrothermal reservoir of Nisyros. To solve this apparent contrast, it must be underscored that R_H values dictated by coexisting anhydrite and pyrite can be attained through gas loss, which determines a retrocession of the progressive evolution of the fluid–rock system towards the full-equilibrium condition.

To investigate the distribution of pH in reservoir fluids, this parameter was computed, in this study, for the liquids feeding the fumarolic vents of Stephanos and Polybote Micros craters, by using the EQ3 code. The adopted procedure is chiefly based on the Cl–δD relation which is constrained by seawater–magmatic water mixing occurring in the roots of the hydrothermal–magmatic system of Nisyros. The temperature variations of these computed pH values are similar to those of theoretical pH buffers, suggesting that some unknown buffer probably control the acidity of reservoir liquids. The pH of the Stephanos liquid varies between 4.72 and 4.85, whereas the pH of the Polybotes Micros liquid changes between 4.88 and 5.23. These pH values are comparable with those of the reservoir liquids encountered by wells Nisyros-1, 5.16, and Nisyros-2, 4.87, but many of them are lower than expected for the full-equilibrium condition. These findings are in contrast with the close attainment of redox equilibrium with the rock buffer throughout the hydrothermal reservoir of Nisyros. To explain this discrepancy, it must be noted that adjustment of the redox potential requires the release of Fe(II) and Fe(III) to the aqueous solution through rock dissolution, which is promoted by acidity-producing species, chiefly CO_2 below 400 °C (Giggenbach, 1993; Reyes et al., 1993; Giggenbach, 1997).

Acknowledgements

References

Akaku, K., Reed, M.H., Yagi, M., Kai, K., Yasuda, Y., 1991. Chemical and physical processes occurring in the Fushime geothermal system, Kyushu, Japan. Geochem. J. 25, 315–333.

Bird, D.K., Schiffman, P., Elders, W.A., Williams, A.E., McDowell, S.D., 1984. Calc-silicate mineralization in active geothermal systems. Econ. Geol. 79, 671–695.

Bohla, M., Keller, J., 1987. Petrology of Plinian eruptions of Nisyros volcano, Hellenic Arc. Terra Cognita 7, 171.

Brombach, T., Hunziker, J.C., Chiodini, G., Cardellini, C., Marini, L., 2001. Soil diffuse degassing and thermal energy fluxes from the southern Lakki plain, Nisyros (Greece). Geophy. Res. Lett. 28, 69–72.

Brombach, T., Caliro, S., Chiodini, G., Fiebig, J., Hunziker, J.C., Raco, B., 2003. Geochemical evidence for mixing of magmatic fluids with seawater, Nisyros hydrothermal system, Greece. Bull. Volcanol. 65, 505–516.

Browne, P.R.L., 1970. Hydrothermal alteration as an aid in investigating geothermal fields. Geothermics 2, 564–570 Spec Issue.

Browne P.R.L. (1977) Hydrothermal alteration in active geothermal fields. N. Z. Geol. Surv., unpublished report M58, 57 pp.

Browne, P.R.L., 1982. Mapping of geothermal discharge features. In: Hochstein, M.P. (Ed.), Introduction to Geothermal Prospecting. Univ. of Auckland Publ, pp. 67–69.

Büttner, A., Kleinhannes, I.C., Rufer, D., Hunziker, J.C., Villa, I.M., 2005. Magma generation at the easternmost section of the Hellenic arc: Hf, Nd, Pb and Sr isotope geochemistry of Nisyros and Yali volcanoes (Greece). Lithos 83, 29–46.

Caliro, S., Chiodini, G., Galluzzo, D., Granieri, D., La Rocca, M., Saccorotti, G., Ventura, G., 2005. Recent activity of Nisyros volcano (Greece) inferred from structural, geochemical and seismological data. Bull. Volcanol. 67, 358–369.

Chiodini, G., Marini, L., 1998. Hydrothermal gas equilibria: The $H_2O–H_2–CO_2–CO–CH_4$ system. Geochim. Cosmochim. Acta 62, 2673–2687.

Chiodini, G., Cioni, R., Guidi, M., Marini, L., 1991. Chemical geothermometry and geobarometry in hydrothermal aqueous solutions: a theoretical investigation based on a mineral-solution equilibrium model. Geochim. Cosmochim. Acta 55, 2709–2727.

Chiodini, G., Cioni, R., Leonis, C., Marini, L., Raco, B., 1993a. Fluid geochemistry of Nisyros island, Dodecanese, Greece. J. Volcanol. Geotherm. Res. 56, 95–112.

Chiodini, G., Cioni, R., Marini, L., 1993b. Reactions governing the chemistry of crater fumaroles from Vulcano Island, Italy, and implications for volcanic surveillance. Appl. Geochem. 8, 357–371.

Chiodini, G., Cioni, R., Marini, L., Panichi, C., 1995. Origin of the fumarolic fluids of Vulcano Island, Italy, and implications for volcanic surveillance. Bull. Volcanol. 57, 99–110.

Chiodini, G., Cioni, R., Frullani, A., Guidi, M., Marini, L., Prati, F., Raco, B., 1996. Fluid geochemistry of Montserrat Island, West Indies. Bull. Volcanol. 58, 380–392.

Chiodini, G., Cioni, R., Guidi, M., Raco, B., Marini, L., 1998. Soil CO_2 flux measurements in volcanic and geothermal areas. Appl. Geochem. 13, 543–552.

Chiodini, G., Frondini, F., Cardellini, C., Granieri, D., Marini, L, Ventura, G., 2001. CO_2 degassing and energy release at Solfatara volcano, Campi Flegrei, Italy. J. Geophys. Res. 106, 16213–16222.

Chiodini, G., Brombach, T., Caliro, S., Cardellini, C., Marini, L., Dietrich, V., 2002. Geochemical indicators of possible ongoing volcanic unrest at Nisyros Island (Greece). Geophys. Res. Lett. 29 (16). doi:10.1029/2001GL014355.

Davis, E., 1967. Zur Geologie und Petrologie der Insel Nisyros und Jali (Dodecanes). Prak. Akad. Athen. 42, 235–252.

Desio A. (1931) Le Isole Italiane dell'Egeo — Studi geologici e geografici-fisici. Memorie descrittive della Carta Geologica d'Italia. R.Ufficio Geologico d'Italia.

Di Paola, G.M., 1974. Volcanology and petrology of Nisyros Island (Dodecanese, Greece). Bull. Volcanol. 38, 944–987.

Dotsika E. (1992) Utilisation du geothermometre isotopique sulfate-eau en milieu de haute temperature sous influence marine potentielle: les systemes geothermaux de Grece. Thèse in Sciences, Université Paris Sud, No 1781.

Dotsika, E., Poutoukis, D., Michelot, J.L., Raco, B., 2009. Natural tracers for identifying the origin of the thermal fluids emerging along the Aegean Volcanic arc (Greece): evidence of Arc-Type Magmatic Water (ATMW) participation. J. Volcanol. Geotherm. Res. 179, 19–32.

Fiebig, J., Chiodini, G., Caliro, S., Rizzo, A., Spangenberg, J., Hunziker, J.C., 2004. Chemical and isotopic equilibrium between CO_2 and CH_4 in fumarolic gas discharges: generation of CH_4 in arc magmatic-hydrothermal systems. Geochim. Cosmochim. Acta 68, 2321–2334.

Francalanci, L., Varekamp, J.C., Vougioukalakis, G., Defant, M.J., Innocenti, F., Manetti, P., 1995. Crystal retention, fractionation and crustal assimilation in a convecting magma chamber, Nisyros Volcano, Greece. Bull. Volcanol. 56, 601–620.

Gansecki C. (1991) Petrology of the domes and inclusions of Nisyros volcano, Dodecanese islands, Greece. BA Thesis, Wesleyan University, Middletown, CT, 97 pp.

Geotermica Italiana (1983) Nisyros 1 geothermal well. Unpublished PPC-EEC report, pp. 106.

Geotermica Italiana (1984) Nisyros 2 geothermal well. Unpublished PPC-EEC report, pp. 44.

Giggenbach, W.F., 1980. Geothermal gas equilibria. Geochim. Cosmochim. Acta 44, 2021–2032.

Giggenbach, W.F., 1984. Mass transfer in hydrothermal alterations systems. Geochim. Cosmochim. Acta 48, 2693–2711.

Giggenbach, W.F., 1987. Redox processes governing the chemistry of fumarolic gas discharges from White Island, New Zealand. Appl. Geochem. 2, 143–161.

Giggenbach, W.F., 1988. Geothermal solute equilibria. Derivation of Na–K–Mg–Ca geoindicators. Geochim. Cosmochim. Acta 52, 2749–2765.

Giggenbach, W.F., 1992. Isotopic shifts in waters from geothermal and volcanic systems along convergent plate boundaries and their origin. Earth Planet. Sci. Lett. 113, 495–510.

Giggenbach, W.F., 1993. Redox control of gas compositions in Philippine volcanic–hydrothermal systems. Geothermics 22, 575–587.

Giggenbach, W.F., 1996. Chemical composition of volcanic gases. In: Scarpa, R., Tilling, R.I. (Eds.), Monitoring and Mitigation of Volcano Hazards. Springer, pp. 221–256.

Giggenbach, W.F., 1997. The origin and evolution of fluids in magmatic-hydrothermal systems, In: Barnes, H.L. (Ed.), Geochemistry of Hydrothermal Ore Deposits, 3d Edition. Wiley, pp. 737–796.

Giggenbach, W.F., Poreda, R.J., 1993. Helium isotopic and chemical composition of gases from volcanic–hydrothermal systems in the Philippines. Geothermics 22, 369–380.

Giggenbach, W.F., Sano, Y., Wakita, H., 1993. Isotopic composition of helium, and CO_2 and CH_4 contents in gases produced along the New Zealand part of a convergent plate boundary. Geochim. Cosmochim. Acta 57, 3427–3455.

Guidi, M., Marini, L., Scandiffio, G., Cioni, R., 1990. Chemical geothermometry in hydrothermal aqueous solutions: the influence of ion complexing. Geothermics 19, 415–441.

Heald, P., Foley, N.K., Hayba, D.O., 1987. Comparative anatomy of volcanic-hosted epithermal deposits: acid-sulfate and adularia–sericite deposits. Econ. Geol. 82, 1–26.

Helgeson, H.C., 1968. Evaluation of irreversible reactions in geochemical processes involving minerals and aqueous solutions: I. thermodynamic relations. Geochim. Cosmochim. Acta 32, 853–877.

Helgeson, H.C., Garrels, R.M., Mackenzie, F.T., 1969. Evaluation of irreversible reactions in geochemical processes involving minerals and aqueous solutions: II. applications. Geochim. Cosmochim. Acta 33, 455–481.

Henley, R.W., Ellis, A.J., 1983. Geothermal systems, ancient and modern: a geochemical review. Earth-Sci. Rev. 19, 1–50.

Innocenti S., Francalanci L., Vougioukalakis G.E. (2002) Changes in the Eruptive Activity of Nisyros, Dodecanese, Greece: Insights from Panagia Kyra' Pyroclastic Series. Am. Geophys. Union Chapman Conf. on Volcanism and the Earth's Atmosphere, The Thera Foundation Conference Center, Santorini, Greece.

Johnson, J.W., Oelkers, E.H., Helgeson, H.C., 1992. SUPCRT 92: a software package for calculating the standard molal thermodynamic properties of minerals, gases, aqueous species, and reactions from 1 to 5000 bars and 0 to 1000 °C. Comput. Geosci. 18, 899–947.

Kassaras, I., Makropoulos, K., Bourova, E., Pedersen, H., Hatzfeld, D., 2005. Upper mantle structure of the Aegean derived from two-station phase velocities of fundamental mode Rayleigh waves. In: Fytikas, M., Vougioukalakis, G.E. (Eds.), The South Aegean Volcanic Arc. : Developments in Volcanology, 7. Elsevier, pp. 19–45.

Keenan, J.H., Keyes, F.G., Hill, P.G., Moore, J.G., 1969. Steam Tables. Thermodynamic Properties of Water Including Vapor, Liquid, and Solid Phases (International System of Units—S.I.). Wiley. 162 pp.

Keller, J., 1971. The major volcanic events in recent eastern mediterranean volcanism and their bearing on the problem of Santorini ash layers. Int. Sci. Congr. Volcano Thera 1, 152–169.

Keller, J., Rehren, T., Stadlbauer, E., 1990. Explosive volcanism in the Hellenic Arc: a summary and review. In: Hardy, D.A., Keller, J., Galanopoulos, V.P., Flemming, N.C., Druitt, T.H. (Eds.), Thera and the Aegean World: Proc. 3d Int. Congr. The Thera Foundation, London, pp. 13–26.

Koutroupis, N., 1983. Geothermal exploration in the Island of Nisyros. Nisyros 1 geothermal well. In: Strub, A.S., Ungemach, P. (Eds.), Proceedings of the Third International Seminar on the Results of EC Geothermal Energy Research. Reidel, Dordrecht, pp. 440–446.

Kristmannsdottir, H., 1982. Alteration in the IRDP drill hole compared with other drillholes in Iceland. J. Geophys. Res. 87, 6525–6531.

Limburg, E.M., Varekamp, J.C., 1991. Young pumice deposits on Nisyros, Greece. Bull. Volcanol. 54, 68–77.

Lodise L. (1987) Petrology and geochemistry of Nisyros volcano (Dodecanese, Greece). MS Thesis, Wesleyan University, Mddletown, CT, USA, 245 pp.

Makris, J., Stobbe, C., 1984. Properties and state of the crust and upper mantle of the eastern Mediterranean Sea deduced from geophysical data. Mar. Geol. 55, 345–361.

Marinelli, G., Marini, L., Merla, A., Sini, R., Ungemach, P., 1983. Geothermal exploration in the island of Nisyros, Dodecanese, Greece. In: Strub, A.S., Ungemach, P. (Eds.), Proceedings of the Third International Seminar on the Results of EC Geothermal Energy Research. Reidel, Dordrecht, pp. 203–205.

Marini, L., Cioni, R., 1985. A chloride method for the determination of the enthalpy of steam/water mixtures discharged from geothermal wells. Geothermics 14, 29–34.

Marini, L., Fiebig, J., 2005. Fluid geochemistry of the magmatic-hydrothermal system of Nisyros (Greece). In: Hunziker, J.C., Marini, L. (Eds.), The Geology, Geochemistry and Evolution of Nisyros Volcano (Greece). Implications for the Volcanic Hazards: Memoires de Géologie (Lausanne), 44, pp. 121–163.

Marini, L., Gambardella, B., 2005. Geochemical modeling of magmatic gas scrubbing. Ann. Geophys. 48, 739–753.

Marini, L., Principe, C., Chiodini, G., Cioni, R., Fytikas, M., Marinelli, G., 1993. Hydrothermal eruptions of Nisyros (Dodecanese, Greece). Past events and present hazard. J. Volcanol. Geotherm. Res. 56, 71–94.

Marini, L., Gambardella, B., Principe, C., Arias, A., Brombach, T., Hunziker, J.C., 2002. Characterization of magmatic sulfur in the Aegean island arc by means of the $\delta^{34}S$ values of fumarolic gases, elemental sulfur, and hydrothermal gypsum of Nisyros and Milos islands. Earth Planet. Sci. Lett. 200, 15–31.

Marini, L., Yock, Fung A., Sanchez, E., 2003a. Use of reaction path modeling to identify the processes governing the generation of neutral Na–Cl and acidic Na–Cl–SO_4 deep geothermal liquids at Miravalles geothermal system, Costa Rica. J. Volcanol. Geotherm. Res. 128, 363–387.

Marini, L., Vetuschi, Zuccolini M., Saldi, G., 2003b. The bimodal pH distribution of volcanic lake waters. J. Volcanol. Geotherm. Res. 121, 83–98.

Martelli A. (1917) Il gruppo eruttivo di Nisiro nel mare Egeo. Società dei XL, ser. 3, XX, 79–165.

Milodowski A.E., Savage D., Bath A.H., Fortey N.J., Nancarrow P.H.A., Shepherd T.J. (1992) Hydrothermal mineralogy in geothermal assessment: studies of the Miravalles field, Costa Rica and experimental simulations of hydrothermal alteration. British Geological Survey Technical Report WE/89/63, Keyworth, Nottingham, 127 pp.

Murray, C., Cubicciotti, D., 1983. Thermodynamics of aqueous sulfur species to 300 °C and potential-pH diagrams. J. Electrochem. Soc. 38, 863–869.

Nordstrom, D.K., Plummer, L.N., Wigley, T.M.L., Wolery, T.J., Ball, J.W., Jenne, E.A., Bassett, R.L., Crerar, D.A., Florence, T.M., Fritz, B., Hoffman, M., Holdren Jr., G.R., Lafon, G.M., Mattigod, S.V., McDuff, R.E., Morel, F., Reddy, M.M., Sposito, G., Thrailkill, J., 1979. A comparison of computerized chemical models for equilibrium calculations in aqueous systems. In: Jenne, E.A. (Ed.), Chemical Modeling in Aqueous Systems: American Chemical Society Symposium Series, 93, pp. 857–892.

Papanikolaou, D.J., Lekkas, E.L., Sakellariou, D., 1991. Geological structure and evolution of the Nisyros Volcano. Bull. Geol. Soc. Greece XXV, 405–419 (In Greek, with English abstract).

Pe-Piper, G., Piper, D.J.W., 2005. The South Aegean active volcanic arc: relationships between magmatism and tectonics. In: Fytikas, M., Vougioukalakis, G.E. (Eds.), The South Aegean Volcanic Arc: Developments in Volcanology, 7. Elsevier, pp. 113–133.

Reed, M.H., 1997. Hydrothermal alteration and its relationship to ore fluid composition, In: Barnes, H.L. (Ed.), Geochemistry of hydrothermal ore deposits, 3d Edition. Wiley, pp. 517–611.

Reyes, A.G., 1990. Petrology of Philippine geothermal systems and the application of alteration mineralogy to their assessment. J. Volcanol. Geotherm. Res. 43, 279–309.

Reyes, A.G., Giggenbach, W.F., Saleras, J.R.M., Salonga, N.D., Vergara, M.C., 1993. Petrology and geochemistry of Alto Peak, a vapor cored hydrothermal system, Leyte Province, Philippines. Geothermics 22, 479–519.

Rochelle, C.A., Milodowski, A.E., Savage, D., Corella, M., 1989. Secondary mineral growth in fractures in the Miravalles geothermal system, Costa Rica. Geothermics 18, 279–286.

Sano, Y., Marty, B., 1995. Origin of carbon in fumarolic gas from island arcs. Chem. Geol. 119, 265–274.

Shimizu, A., Sumino, H., Nagao, K., Notsu, K., Mitropoulos, P., 2005. Variation in noble gas isotopic composition of gas samples from the Aegean arc, Greece. J. Volcanol. Geotherm. Res. 140, 321–339.

St. Seymour, K., Vlassopoulos, D., 1992. Magma mixing at Nisyros volcano, as inferred from incompatible trace-elements systematics. J. Volcanol. Geotherm. Res. 50, 273–299.

Steiner, A., 1977. The Wairakei geothermal area, North Island, New Zealand. N. Z. Geol. Surv. Bull. 90 136 pp.

Symonds, R.B., Gerlach, T.M., Reed, M.H., 2001. Magmatic gas scrubbing: implications for volcano monitoring. J. Volcanol. Geotherm. Res. 108, 303–341.

Vanderkluysen L., Volentik A. (2002) Volcanological and Petrological Evolution of the Volcanic Island of Nisyros, Greece. Master's (DEA) Thesis, Université de Lausanne, 200 pp.

Vanderkluysen, L., Volentik, A., Hernandez, J., Hunziker, J.C., Bussy, F., Principe, C., 2005a. The petrology and geochemistry of lavas and tephras of Nisyros Volcano (Greece). In: Hunziker, J.C., Marini, L. (Eds.), The Geology, Geochemistry and Evolution of Nisyros Volcano (Greece). Implications for the Volcanic Hazards: Memoires de Géologie (Lausanne), 44, pp. 79–99.

Vanderkluysen, L., Volentik, A., Principe, C., Hunziker, J.C., Hernandez, J., 2005b. Nisyros' volcanic evolution: the growth of a strato-volcano. In: Hunziker, J.C., Marini, L. (Eds.), The Geology, Geochemistry and Evolution of Nisyros Volcano (Greece). Implications for the Volcanic Hazards: Memoires de Géologie (Lausanne), 44, pp. 100–106.

Volentik, A., Vanderkluysen, L., Principe, C., Hunziker, J.C., 2002. Stratigraphy of the caldera walls of Nisyros volcano, Greece. Eclogae Geol. Helv. 95, 223–235.

Volentik, A., Principe, C., Vanderkluysen, L., Hunziker, J.C., 2005a. Explanatory notes on the "Geological Map of Nisyros Volcano (Greece)". In: Hunziker, J.C., Marini, L. (Eds.), The Geology, Geochemistry and Evolution of Nisyros Volcano (Greece). Implications for the Volcanic Hazards: Memoires de Géologie (Lausanne), 44, pp. 7–25.

Volentik, A., Vanderkluysen, L., Principe, C., Hunziker, J.C., 2005b. Stratigraphy of Nisyros Volcano (Greece). In: Hunziker, J.C., Marini, L. (Eds.), Memoires de Géologie (Lausanne), 44, pp. 26–66.

Volentik, A., Vanderkluysen, L., Principe, C., Hunziker, J.C., 2005c. The role of tectonic and volcano-tectonic activity at Nisyros Volcano (Greece). In: Hunziker, J.C., Marini, L. (Eds.), The Geology, Geochemistry and Evolution of Nisyros Volcano (Greece). Implications for the Volcanic Hazards: Memoires de Géologie (Lausanne), 44, pp. 67–78.

Vougioukalakis G. E. (1984) Studio vulcanologico e chimico-petrografico dell'isola di Nisyros (Dodecanneso, Grecia). Tesi di laurea, Università di Pisa.

Vougioukalakis, G.E., 1993. Volcanic stratigraphy and evolution of Nisyros Island. Bull. Geol. Soc. Greece XXVII, 239–258 (In Greek, with English abstract).

Vougioukalakis G.E. (1998) Blue volcanoes: Nisyros. Regional Council of Mandraki.

Vrouzi, F., 1985. Research and development of geothermal resources in Greece: present status and future prospects. Geothermics 14, 213–227.

Wolery, T.W., Jarek, R.L., 2003. Software User's Manual. EQ3/6, Version 8.0. Sandia National Laboratories — U.S. Dept. of Energy Report.

Wyers, G.P., Barton, M., 1989. Polybaric evolution of calc-alkaline magmas from Nisyros, Southeastern Hellenic Arc, Greece. J. Petrol. 30, 1–37.